This is the accepted manuscript made available via CHORUS. The article has been published as:

Slow spin relaxation in single endohedral fullerene molecules

Jie Li, Lei Gu, and Ruqian Wu

Phys. Rev. B **104**, 224431 — Published 28 December 2021

DOI: 10.1103/PhysRevB.104.224431

Slow Spin Relaxation in Single Endohedral Fullerene Molecules

Jie Li, Lei Gu and Ruqian Wu*

Department of Physics and Astronomy, University of California, Irvine, California 92697-4575, USA.

ABSTRACT: Well-protected magnetization, tunable quantum states and long spin relaxation time are desired for the use of magnetic molecules in spintronics and quantum information technologies. In this work, endohedral fullerene molecules M@C_{28} with different transition metal cores were explored through systematic first-principles calculations and spin dynamics analyses. Many of them have bias-tunable structure, stable magnetization, and sizeable magnetic anisotropy energy. Furthermore, some of them may have spin relaxation time up to several milliseconds for their quantum spin states at high temperature (~10K) after full consideration of spin-vibration couplings. Our results suggest that these M@C_{28} provide a rich pool of single-molecule magnets for diverse applications.

* E-mail: wur@uci.edu.

I. INTRODUCTION

The foremost important issue for using magnetic molecules as units in spin filtering, quantum computing and magnetic sensing devices is to have a long coherence time [1-3]. For example, well characterized quantum states and long coherence times are among the critical prerequisites proposed by DiVincenzo for qubits [4]. It is recognized that spins in a magnetic molecule may provide quantum states with energy splittings in the microwave range for quantum computation and hence research interest in magnetic molecules has noticeably surged in recent years [5-9]. Different strategies have been proposed for the design of magnetic molecules with large spin relaxation time (τ), from single core magnetic molecules [9-10], to multiple core magnetic clusters [11-13]. In general, spin relaxation time has an activated Arrhenius-like behavior at a high temperature: i.e., $\tau = \tau_0 e^{U_{eff}/k_B T}$, where τ_0 represents the inverse attempt frequency, and U_{eff} and k_B are the effective barrier for relaxation and the Boltzmann constant, respectively [14]. Without the vibration-assisted tunneling effect, U_{eff} is solely determined by the magnetic anisotropy energy (MAE). This inspired an active search for molecules with enhanced MAEs, using low-symmetry structures [15-18] and heavy elements including rare earth and actinide atoms [19-21]. Nevertheless, recent studies indicated that spin-vibration coupling, hyperfine interaction, and intermolecular interaction may even more significantly affect the quantum coherence of magnetic molecules [22], particularly when their MAEs are high. It is critical to establish roles of different factors in the molecular quantum decoherence and, as a further step, to find molecules with long relaxation time through the manipulation of magnetization, spin orbit coupling and spin-vibration coupling (SVC).

In this work, we systematically investigate the spin relaxation in a series of bias-controllable magnetic endohedral fullerenes: M@C_{28} (M=3d, 4d and 5d transition metals), through a

combination of density functional calculations and spin dynamics simulations. Several such endohedral fullerenes (e.g., Ti@C_{28}, Zr@C_{28}, and U@C_{28}) have already been synthesized in recent experiments [23] and hence there should be no prohibitive technological barrier for developing similar molecules if attractive properties are predicted. The closed mesh topology of fullerene shells offers a protective environment for magnetic atoms and reduce spin-vibration coupling, especially for the low energy modes. We find that these endohedral fullerenes have various attractive properties such as structural bistability, ferroelectricity, multiple magnetic phases with large MAEs. Furthermore, some of them have long spin relaxation time for their low-energy Kramers doublets, up to the millisecond order even at a temperature of ~10 K. These findings suggest a possibility of designing single magnetic molecules for diverse applications.

II. METHODOLOGY

All ab initio calculations in this work were carried out with the Vienna ab-initio simulation package (VASP) at the level of the spin-polarized generalized-gradient approximation (GGA) [24]. The interaction between valence electrons and ionic cores was considered within the framework of the projector augmented wave (PAW) method [25,26]. The energy cutoff for the plane wave basis expansion was set to 500 eV. A Hubbard U_{eff} = U-J = 2.0 eV within the Dudarev scheme was added to take account of the onsite coulomb interaction for transition metals atom d orbitals [27] (see the effect of different U values in Fig. S1). All atoms were fully relaxed using the conjugated gradient method for the energy minimization until the force on each atom became smaller than 0.01 eV/Å, and 10^{-6} as the convergence criteria for total energy was selected for all DFT calculations. The density functional perturbation theory is carried out within the density functional framework to calculate the vibrational properties [28]. The spin-vibration dynamics and the spin-spin dynamics

calculations were simulated by using the master equations with DFT parameters, (see details in the Supplemental Material [29]).

III. RESULTS AND DISCUSSION

C_{28} has a tetrahedral structure as Fig. 1, with three pentagons directly fused on the dome [30]. Experimental investigations indicated that C_{28} can be stabilized by insertion of appropriate core atom [23]. To show their dynamic stability, we performed ab initio molecular dynamics (AIMD) simulations at 300K for 10 ps for Ir@C_{28} and Rh@C_{28} molecules. As shown in videos in supplemental material [29], we found that their structures are not noticeably deformed after a few thousand MD steps and the energy fluctuates in a narrow range (cf. Fig. S2). Therefore, we may reasonably assume that many endohedral C28 fullerenes can be synthesized.

Our density functional theory (DFT) calculations indicate that most gas-phase M@C_{28} molecules (M= 3d, 4d and 5d transition metals) have two structural phases (denoted as I and II below), both with a C_3 symmetry as shown in Fig. 1. The displacements of M atoms between the two phases are shown in Table 1. Using Ir@C_{28} as an example, Ir atom displaces by 1.1 Å as the phase changes and the C_{28} cage also deforms slightly, i.e., the aspect ratios (height vs. width) change from 0.860 in the pristine C_{28} to 0.923 (phase I) and 0.996 (phase II), respectively. The planar average charge density difference in Fig. 1 shows that electrons transfer from Iridium to carbon atoms. The Bader charge of Iridium atom is -1.1e (phase I) or -0.9e (phase II), and charge redistribution is detailed in Fig. S3 [29]. The separation of positive and negative charge centers gives rise to dipole moments of 0.326eÅ and -0.701eÅ in these two phases. In Table I, one may see that dipole moments of all M@C_{28} are nonzero. This offers a possibility for gate control between their phases and possibly strong response to microwave manipulation especially in the THz regime.

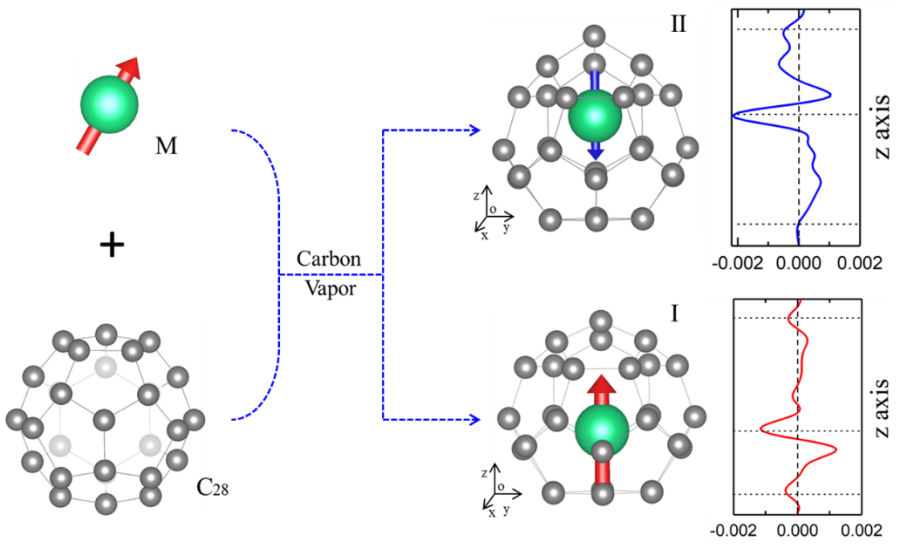


FIG. 1. (Left) Schematic diagram of the synthesis process of M@C_{28} in two phases (I and II) (Red and blue arrows represent the direction of the dipoles). (Right) The corresponding charge difference of Ir@C_{28}, i.e., in I and II phases, respectively. (Positive and negative represent charge accumulation and depletion, respectively).

It is desired to have large MAEs, as the first step, to search magnetic molecules with long spin relaxation time. Systematic DFT calculations show that most of M@C_{28} are magnetic except for the Ti, Zr and Hf cases as shown in Fig. 2a. Taking Ir@C_{28} as the example, one may see a strong hybridization between Ir and C_{28} orbitals from the curves of projected density of states (PDOS) of Ir@C_{28} in Fig. 2b. Significant spin-polarization is also induced around C atoms, especially for those next to Ir as shown by the spin density in insets of Fig. 2b. Quantitatively, the total magnetic moments of Ir@C_{28} are 5.0 μ_B and 1.0 μ_B in phases I and II, for which C atoms contribute 1.82μ_B and 0.46μ_B, respectively. The relatively nonlocal magnetization in the carbon cage may induce weak spin polarization in supporting substrates such as graphene and hence offers a possibility to establish quantum entanglement among magnetic molecules. For example, a gate may control the density of carriers or energy alignment in supporting materials through which the long-range magnetic coupling between molecules can be either established or eliminated.

Table I. The displacements (Δu) of M atoms between phase transition and the difference of electric dipole moments ($\Delta D = D_I - D_{II}$, where D_I and D_{II} represent their electric dipole moments in phase I and II, respectively) of M@C_{28}.

	Ti	V	Cr	Mn	Fe	Co	Ni
Δu (Å)	0.93	1.04	1.06	0.95	0.63	1.00	0.81
ΔD(eÅ)	0.92	0.78	0.91	0.66	0.40	0.61	0.44
	Zr	Nb	Mo	Tc	Ru	Rh	Pd
Δu (Å)	0.02	0.20	0.83	1.08	1.02	0.47	0.39
ΔD(eÅ)	0.01	0.46	0.80	1.46	1.34	0.48	0.32
	Hf	Ta	W	Re	Os	Ir	Pt
Δu (Å)	0.01	0.72	1.03	1.13	0.98	1.10	0.38
ΔD(eÅ)	0.01	0.61	0.64	0.95	1.37	1.02	0.33

To determine their MAEs, we calculate the torque *T(θ)* as a function of the polar angle θ between the magnetization and the z-axis. The torque is defined as [31,32],

$$T(\theta) = \frac{dE(\theta)}{d\theta} = \sum_{occ} \left\langle \psi_{jk} \middle| \frac{\partial H_{so}}{\partial \theta} \middle| \psi_{jk} \right\rangle \quad (1)$$

with the spin-orbit coupling Hamiltonian $H_{so} = \sum_i \xi_i \hat{l}_i \cdot \hat{s}_i$ with $\hat{l}_i = -ir_i \times \nabla$. The indices *i* and *j* refer to individual atoms and eigenstates, and the summation in Eq. 1 goes over all occupied states. By integrating *T(θ)*, we may obtain the total energy $E(\theta)$ as a function of the polar angle θ, and the MAEs equal to the energy differences between the lowest and highest energies. In Fig. 2c, Ir@C_{28} has the lowest and highest energies occurring at θ=0° and θ=90°, indicating that its easy axis is along the z-axis for both phase I and phase II. Nevertheless, the energy differences, $MAE = E(\theta = 90°) - E(\theta = 0°)$, drastically differ, from 32.2 meV for the phase I to only 0.93meV for the phase II. To assess the tunability of this important parameter, we further calculate the Fermi level dependences of total and spin channel decomposed MAEs according to the rigid band model

[31,33] and results are shown in Fig. 2d. For both cases, the MAE curves are flat in a broad energy range around the Fermi level, but the MAE of the phase I may drop to a large negative value as the Fermi level moves down by 0.2 eV. This is because that the Fermi level skips through the hybridized d_{z^2} orbital of Ir. In Fig. 2a, one may see that the 5d (4d) cores lead to larger MAEs than 4d (3d) cores by an order of magnitude. As we need molecules with large positive MAEs for applications, we choose Rh@C_{28} and Ir@C_{28} in phase I as examples for spin dynamic studies.

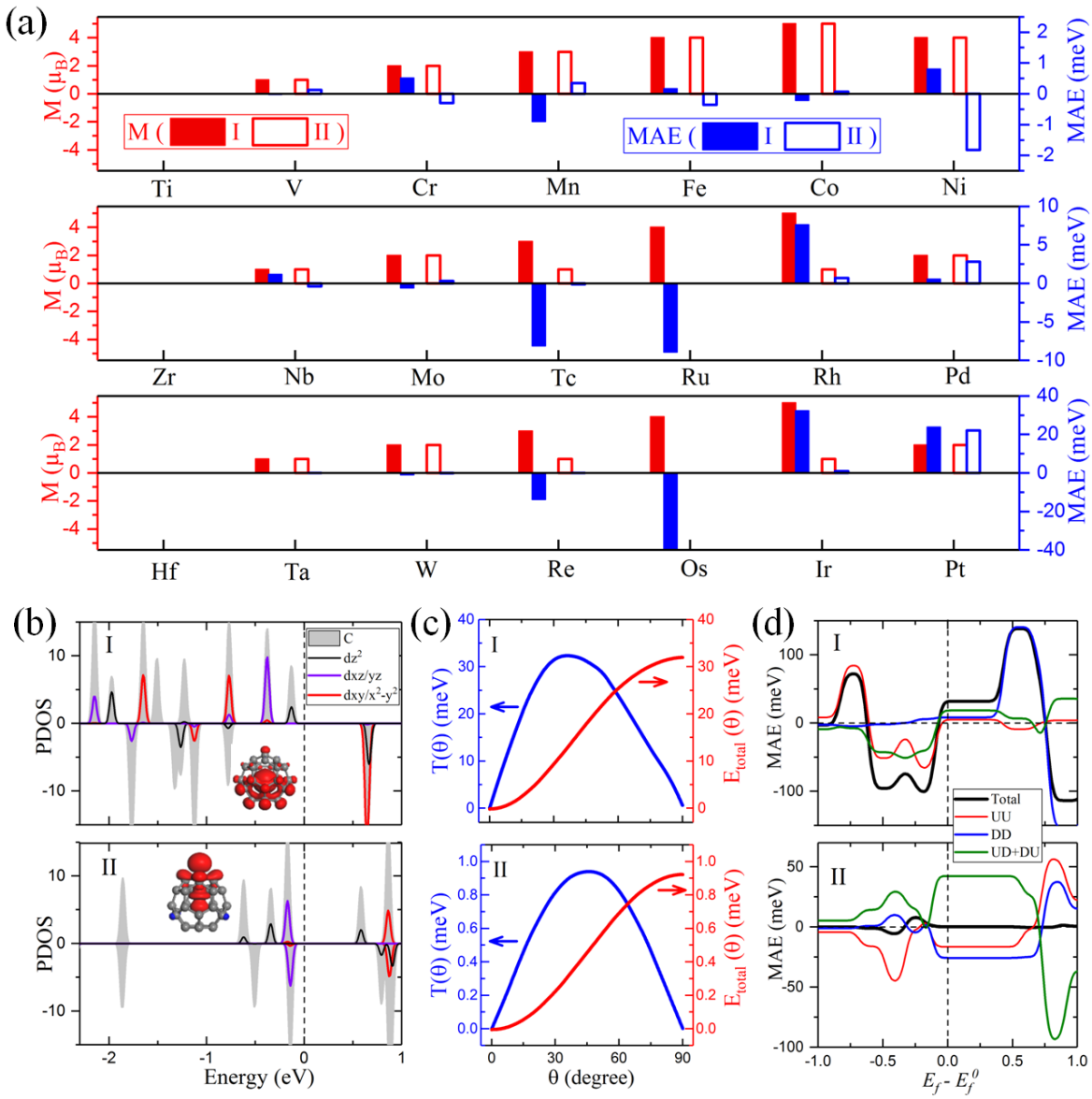


FIG. 2. (a) The calculated magnetic moments and MAEs of M@C_{28} (M= 3d, 4d and 5d transition metals). (b) The PDOS of Ir@C_{28} in two phases (inset are the corresponding spin density). (c)

Calculated torque vs the angle θ for Ir@C_{28}. (d) The Fermi level dependent total and spin channel decomposed MAEs of Ir@C_{28} from the rigid band model analyses.

To describe quantum states of these magnetic molecule, we introduce a spin Hamiltonian as

$$H_{spin} = -D_{xx}S_x^2 - D_{yy}S_y^2 - D_{zz}S_z^2 - D_{xy}(S_xS_y + S_yS_x)$$
$$-D_{xz}(S_xS_z + S_zS_x) - D_{yz}(S_yS_z + S_zS_y) \quad (2)$$

where the magnetic anisotropy is extended to a D-tensor. These parameters are computed by the four-state mapping method [34]:

$$D_{\alpha\beta} = \frac{-1}{4S^2}(E_{\alpha\beta}^1 + E_{\alpha\beta}^4 - E_{\alpha\beta}^2 - E_{\alpha\beta}^3) \quad (3)$$

In which $E_{\alpha\beta}^{1-4}$ are the energies of four different spin configurations (see details in the Supplemental Material [29]). For a magnetic molecule with large D_{zz}, the energy diagram is sketched in Fig. 3(a). Since the MAE is high and so is the separation between different doublets, we may concentrate on the relaxation of the ground state doublet due to the SVC.

According to Eq. 2, the SVC is caused by vibration-induced changes of D parameters. Here, we investigate the effects of both the first- and second-order SVC coefficients on the spin decoherence. The first-order SVC coefficients can be obtained by taking the derivatives of Eq. 2 with respect to $u_{i\gamma}$ (the displacements of atom *i* along γ direction):

$$\frac{\partial H_{spin}}{\partial u_{i\gamma}} = \sum_{\alpha\beta} \frac{-\partial D_{\alpha\beta}}{\partial u_{i\gamma}} S_{\alpha\beta}^2 \quad (4)$$

with

$$\frac{\partial D_{\alpha\beta}}{\partial u_{i\gamma}} = \frac{-1}{4S^2}\left(\frac{\partial E_{\alpha\beta}^1}{\partial u_{i\gamma}} + \frac{\partial E_{\alpha\beta}^4}{\partial u_{i\gamma}} - \frac{\partial E_{\alpha\beta}^2}{\partial u_{i\gamma}} - \frac{\partial E_{\alpha\beta}^3}{\partial u_{i\gamma}}\right) \quad (5)$$

where, $-\frac{\partial E_{\alpha\beta}^n}{\partial u_{i\gamma}}$ (n=1,…,4) denotes the force acting on the atom *i* along the γ direction. The second-order SVC coefficients can be expressed as:

$$\frac{\partial^2 H_{spin}}{\partial u_{i\gamma}\partial u_{i'\gamma'}} = \sum_{ij} \frac{-\partial^2 D_{\alpha\beta}}{\partial u_{i\gamma}\partial u_{i'\gamma'}} S_{\alpha\beta}^2 \quad (6)$$

with

$$\frac{\partial^2 D_{\alpha\beta}}{\partial u_{i\gamma}\partial u_{i'\gamma'}} = \frac{-1}{4S^2}\left(\frac{\partial^2 E^1_{\alpha\beta}}{\partial u_{i\gamma}\partial u_{i'\gamma'}} + \frac{\partial^2 E^4_{\alpha\beta}}{\partial u_{i\gamma}\partial u_{i'\gamma'}} - \frac{\partial^2 E^2_{\alpha\beta}}{\partial u_{i\gamma}\partial u_{i'\gamma'}} - \frac{\partial^2 E^3_{\alpha\beta}}{\partial u_{i\gamma}\partial u_{i'\gamma'}}\right) \quad (7)$$

In the DFT schemes with the plane wave bases, $-\frac{\partial E^n_{\alpha\beta}}{\partial u_{i\gamma}}$ and $\frac{\partial^2 E^n_{\alpha\beta}}{\partial u_{i\gamma}\partial u_{i'\gamma'}}$ (n=1,…,4) are connected to the Hellmann-Feynman forces and the Hessian matrices, respectively. The calculated vibration modes and energies of Rh@C_{28} and Ir@C_{28} in gas phase in the 0-50 meV range as shown in Fig. 3b. One can see that two lowest vibrations modes are in-plane, while the third one is along the z axis.

The dynamics of the quantum spin states can then be described by the master equation:

$$\frac{dp_m(t)}{dt} = \sum_n (p_n(t)q_{nm} - p_m(t)q_{mn}) \quad (8)$$

where p_m represent the probability of being at quantum spin states $|m\rangle$ and q_{mn} represent the transition rate from quantum spin states $|m\rangle$ to $|n\rangle$. The magnetic relaxation pathways for a ground state doublet are those illustrated schematically in Fig. 3a, where both the Orbach and Raman processes are included. By using the master equations with DFT parameters [35-41], (see details in the Supplemental Material [29], see, also, references [35, 36, 42] therein), the probabilities of holding in the Kramers doublets of Ir@C_{28} through relaxation are shown in Fig. 3c. While the excited doublet quickly decays (within 10^{-4} ms as shown in the inset), the ground state doublet decay rather slowly. One may see from Fig. 3c that a long spin-lattice relaxation time T_1 (2.3ms) can be achieved at a reasonably high temperature (10K) for the ground state doublet of Ir@C_{28}. For Rh@C_{28} with weaker SOC, the SVC is weaker as well and the spin-lattice relaxation time T_1 is 0.7ms. Both of them exceed the time scale for coherent manipulations of the electron spin (~10ns based on the existing apparatus) [43]. We would hope that our work may inspire experimental

interest to synthesize Ir@C_{28} or Rh@C_{28} as they are promising for applications.

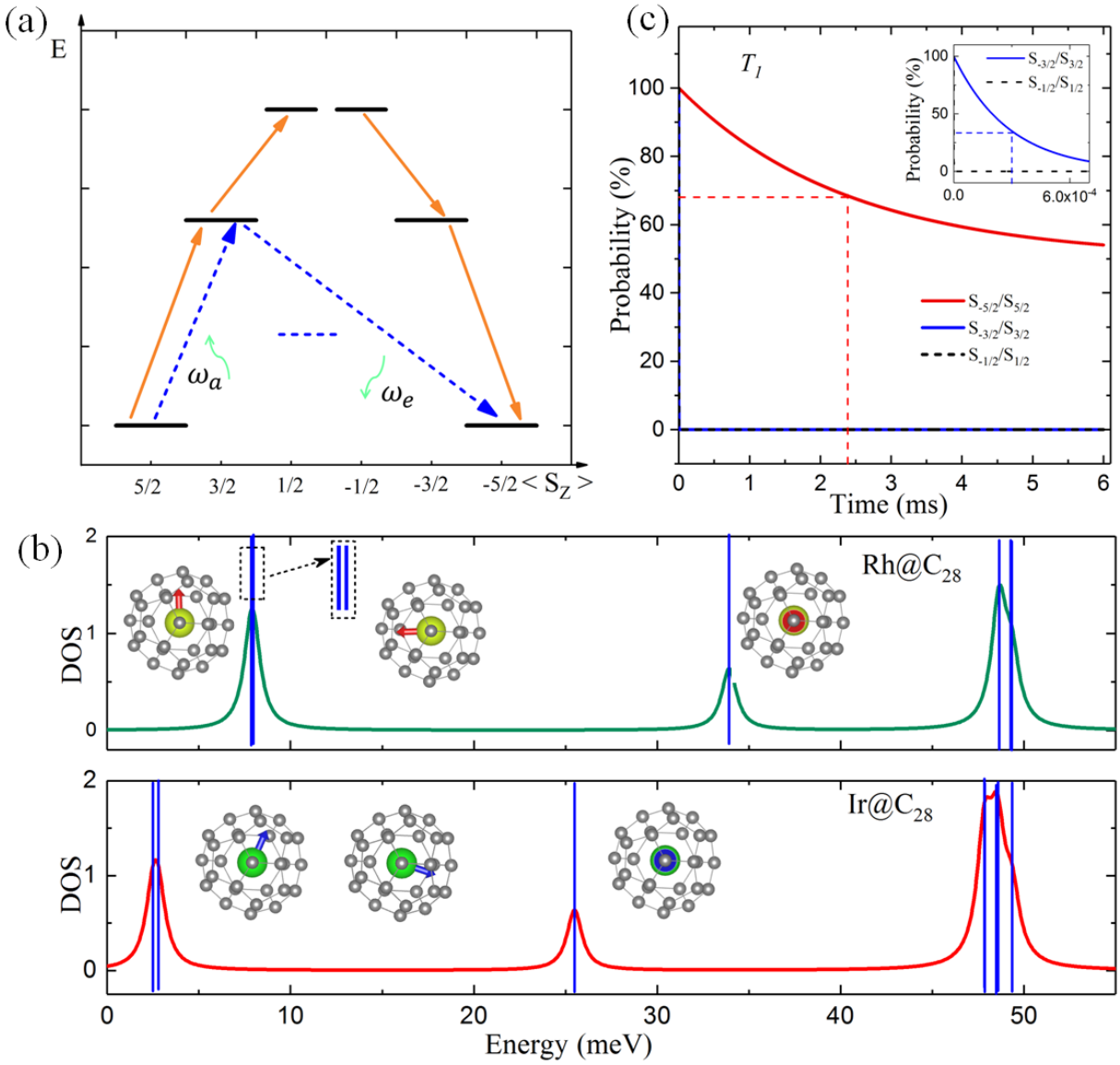


FIG. 3. (a) Schematics of the magnetic relaxation processes of spin states. The solid orange and dash blue arrows represent the Orbach process and Raman process; ω_a and ω_e represent the vibrational absorption and emission, respectively. The horizontal blue dashed line is a virtual state. (b) The phonon DOS of Rh@C_{28} and Ir@C_{28} with energies smaller than 50 meV from broadening of local vibrational modes (The blue lines are their corresponding vibration spectrum in gas phase). (c) The decaying of quantum spin states of Ir@C_{28} in phase I (S=5/2) with time at a reasonably high temperature (10K). The top right inset is the corresponding zoom-in decaying of the $S_{-3/2}/S_{3/2}$ and $S_{-1/2}/S_{1/2}$ in T_1 mechanism.

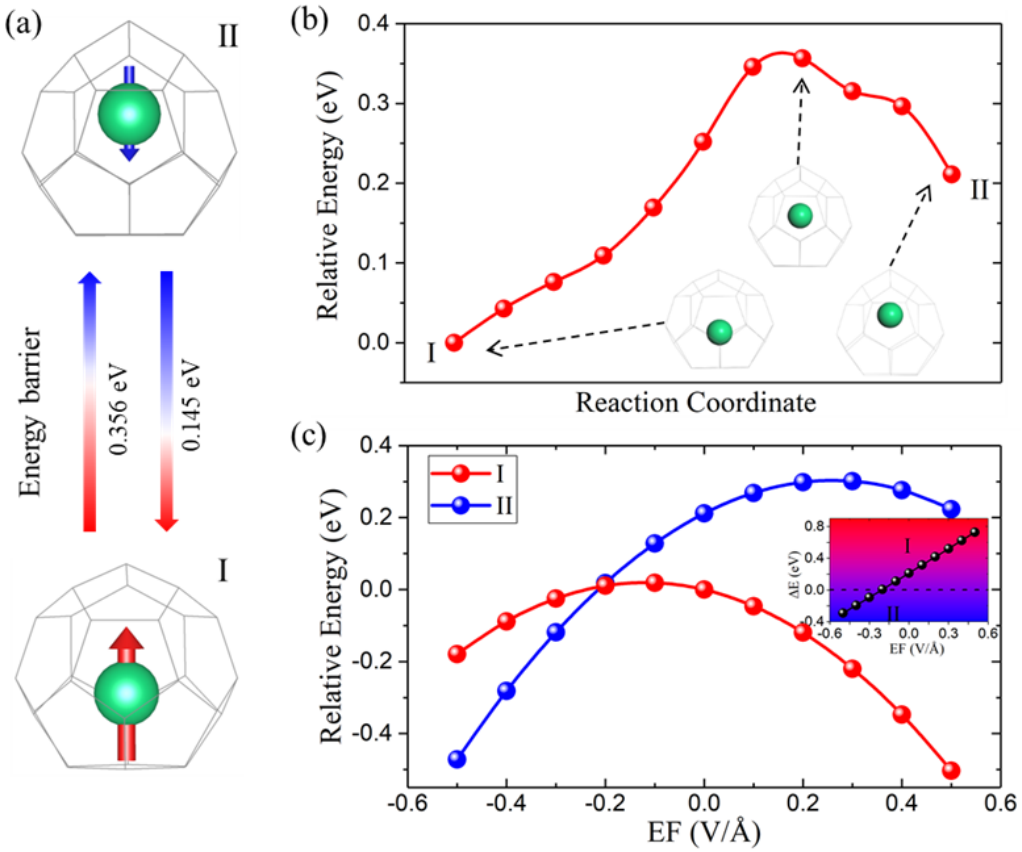


FIG. 4. (a) Schematic diagram of the switching between the phases I and II of Ir@C_{28} (Red and blue arrows are represent the direction of the dipoles). (b) Energetics pathway for structural transition and the optimized structures for Ir@C_{28} in phases I and II and the transition state between them. (c) The relative energy of Ir@C_{28} in phases I and II as functions of the external electric field (negative external electric field is along z axis).

The other advantage of M@C_{28} is that it has two stable phases with distinctly different quantum states as shown in Fig. 4a. From climbing image nudged elastic band (CINEB) calculations with 9 intermediate images between phases I and II, one may see that phase I (II) of Ir@C_{28} has an energy barrier of ~ 0.356eV (0.145eV) in the switching process (see in Fig.4b). As Ir is ionized in the carbon cage, an external electric field may drive the phase transition. From the calculated total energies under an external electric field in Fig. 4c, one may convert Ir@C_{28} from

phase I to phase II by applying a reasonable electric field of 0.2V/Å. We may then tune the potential molecules in an array into different phases, as illustrated for two in Fig. S5 [29]. Graphene or silicon can be adopted as the substrate and Au electrodes can be buried underneath for gate bias.

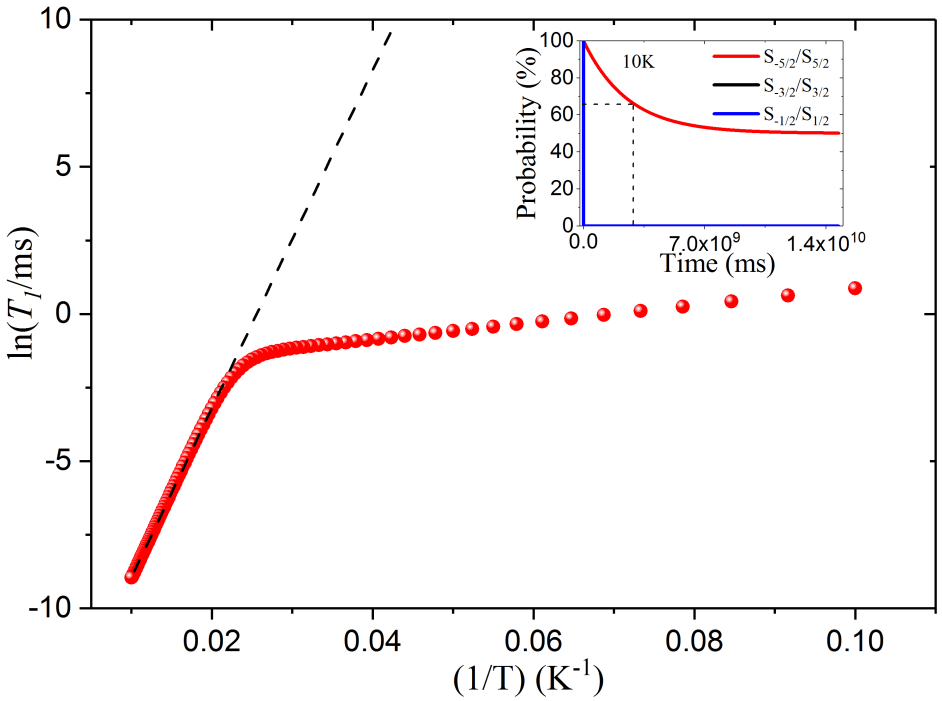


FIG. 5. The spin relaxation time as functions of temperature (the black dashed line is the Orbach barrier). The top right inset is the decaying of the ground state doublet of Ir@C_{28} with only the Orbach processes being considered in the T_1 mechanism (the spin-lattice relaxation) at 10K.

Note that Rh@@C_{28} has smaller MAE and weaker SVC but has a similar relaxation time as Ir@C_{28}. This shows that large MAE and weak SVC are the two equally important factors for the spin relaxation time of single magnetic molecules. Therefore, another strategy for the design of single-molecule magnets and qubits is to reduce the spin-vibration coupling. Meanwhile, our calculations show that the Orbach processes is much less important compared to the Raman processes for the spin relaxation at low temperature. For example, T_1 of the ground state doublet of Ir@C_{28} in the inset of Fig. 5 can be up to ~2.6×10^9 ms if only the Orbach processes are

considered at 10K. As the temperature increasing, the role of the Orbach processes will be furtherly enhanced, and the relaxation time then will have an Arrhenius behavior, as depicted in Fig. 5. Therefore, the Raman processes are dominant in the determination of relaxation time of the ground state doublet a reasonably low temperature, especially for the magnetic molecules with large MAEs. Compared to other endohedral fullerenes, e.g., paramagnetic $N@C_{60}$ and $P@C_{60}$ molecules [44-46], the large MAE of Ir or Rh encapsulated C_{28} may have reasonably high blocking temperature in the absence of high external magnetic field. While this work lays a conceptual groundwork, much more needs to be done for the actual use of endohedral fullerene molecules in quantum information and spintronic technologies, of course. Some other detrimental factors such as hyperfine interaction, intermolecular interaction and substrate effect should be examined.

IV. CONCLUSION

In summary, we proposed that several endohedral fullerene molecule $M@C_{28}$ can have long spin relaxation time with full consideration of SVC, and hence can be developed for diverse applications such as spin filtering and quantum sensing. The closed mesh topology of C_{28} offers a protective and low-symmetry environment for the magnetic atom, yet adequate exchange interaction among molecules for electric manipulation and the establishment of quantum entanglement. They also have sizeable electric dipole moments and dual stability, a leeway for bias control in quantum operations.

Acknowledgements

Authors thank Profs. W. Ho and W. Evans at the University of California Irvine for insightful

discussions. This work was supported by US DOE, Basic Energy Science (Grant No. DE-SC0019448). Calculations were performed on parallel computers at NERSC.

REFERENCES

[1] M. N. Leuenberger, and D. Loss, Quantum computing in molecular magnets, Nature **410**, 789 (2001).

[2] A. Ardavan, O. Rival, J. J. L. Morton, S. J. Blundell, A. M. Tyryshkin, G. A. Timco, and R. E. P. Winpenny, Will spin-relaxation times in molecular magnets permit quantum information processing? Phys. Rev. Lett. **98**, 057201(2007).

[3] C. Schlegel, J. van Slageren, M. Manoli, E. K. Brechin, and M. Dressel, Direct observation of quantum coherence in single-molecule magnets, Phys. Rev. Lett. **101**, 147203 (2008).

[4] D. DiVincenzo, The physical implementation of quantum computation, Fortschritte der Physik. **48**, 771 (2000).

[5] K. Bader, D. Dengler, S. Lenz, B. Endeward, S. Jiang, P. Neugebauer, and J. Slageren, Room temperature quantum coherence in a potential molecular qubit, Nat Commun. **5**, 5304 (2014).

[6] M. Atzori, L. Tesi, E. Morra, M. Chiesa, L. Sorace, and R. Sessoli, Room-temperature quantum coherence and rabi oscillations in vanadyl phthalocyanine: toward multifunctional molecular spin qubits, J. Am. Chem. Soc. **138**, 2154 (2016).

[7] E. Coronado, Molecular magnetism: from chemical design to spin control in molecules, materials and devices, Nat Rev Mater. **5**, 87 (2020).

[8] E. Garlatti, L. Tesi, A. Lunghi, M. Atzori, D. J. Voneshen, P. Santini, S. Sanvito, T. Guidi, R. Sessoli, and S. Carretta, Unveiling phonons in a molecular qubit with four-dimensional inelastic neutron scattering and density functional theory, Nat Commun. **11**, 1751 (2020).

[9] J. Chen, C. Hu, J. F. Stanton, S. Hill, H. Cheng, and X. G. Zhang, Decoherence in molecular electron spin qubits: insights from quantum many-body simulations, J. Phys. Chem. Lett. **11(6)**, 2074 (2020).

[10] J. M. Zadrozny, J. Niklas, O. G. Poluetkov, and D. E. Freedman, Millisecond coherence time in a tunable molecular electronic spin qubit, ACS Cent. Sci. **1**, 488 (2015).

[11] S. Bertaina, S. Gambarelli, T. Mitra, B. Tsukerblat, A. Müller, and B. Barbara, Quantum oscillations in a molecular magnet, Nature **453**, 203 (2008).

[12] Z. Hu, B. Dong, Z. Liu, J. Liu, J. Su, C. Yu, J. Xiong, D. Shi, Y. Wang, B. W. Wang, A. Ardavan, Z. Shi, S.D. Jiang, and S. Gao, Endohedral Metallofullerene as Molecular High Spin

Qubit: Diverse Rabi Cycles in $Gd_2@C_{79}N$, J. Am. Chem. Soc. **140**, 1123 (2018).

[13] M. Mannini, F. Pineider, C. Danieli, F. Totti, L. Sorace, Ph. Sainctavit, M. A. Arrio, E. Otero, L. Joly, J. C. Cezar, A. Cornia, and R. Sessoli, Quantum tunnelling of the magnetization in a monolayer of oriented single-molecule magnets, Nature **468**, 417 (2010).

[14] D. Gatteschi, R. Sessoli, and J. Villain, Molecular nanomagnets, Mesoscopic Physics and Nanotechnology. (OUP Oxford, **2006**).

[15] T. O. Strandberg, C. M. Canali, and A. H. Macdonald, Transition-metal dimers and physical limits on magnetic anisotropy, Nat. Mater. **6**, 648 (2007).

[16] R. Xiao, D. Fritsch, M. D. Kuz'min, K. Koepernik, H. Eschrig, M. Richter, K. Vietze, and G. Seifert, Co dimers on hexagonal carbon rings proposed as subnanometer magnetic storage bits, Phys. Rev. Lett. **103**, 187201 (2010).

[17] J. Hu, and R. Wu, Giant magnetic anisotropy of transition-metal dimers on defected graphene, Nano Lett. **14**, 1853 (2014).

[18] I. G. Rau, S. Baumann, S. Rusponi, F. Donati, S. Stepanow, L. Gragnaniello, J. Dreiser, C. Piamonteze, F. Nolting, S. Gangopadhyay, O. R. Albertini, R. M. Macfarlane, C. P. Lutz, B. A. Jones, P. Gambardella, A. J. Heinrich, and H. Brune, Reaching the magnetic anisotropy limit of a 3d metal atom, Science **344**, 988 (2014).

[19] K. S. Pedersen, A. Ariciu, S. McAdams, H. Weihe, J. Bendix, F. Tuna, and S. Piligkos, Toward molecular 4f single-ion magnet qubits, J. Am. Chem. Soc. **138**, 5801 (2016).

[20] S. Bertaina, S. Gambarelli, A. Tkachuk, I. N. Kurkin, B. Malkin, A. Stepanov, and B. Barbara, Rare-earth solid-state qubits, Nat. Nanotechnol. **2**, 39 (2007).

[21] J. Li, L. Gu, and R. Q. Wu, Giant magnetic anisotropy energy and long coherence time of uranium substitution on defected Al_2O_3(0001), Phys. Rev. B **102**, 054406 (2020).

[22] A. Gaita-Arino, F. Luis, and E. Coronado, Molecular spins for quantum computation, Nat. Chem. **11**, 301 (2019).

[23] P. W. Dun, N. K. Kaiser, M. Mulet-Gas, A. Rodríguez-Fortea, J. M. Poblet, H. Shinohara, C. L. Hendrickson, A. G. Marshall, H. W. Kroto, The smallest stable fullerene, $M@C_{28}$ (M = Ti, Zr, U): stabilization and growth from carbon vapor, J. Am. Chem. Soc. **134**, 9380 (2012).

[24] P. E. Blochl, Projector augmented-wave method, Phys. Rev. B **50**, 17953 (1994).

[25] G. Kresse, and D. Joubert, From ultrasoft pseudopotentials to the projector augmented-wave

method, Phys. Rev. B **59**, 1758 (1999).

[26] J. P. Perdew, K. Burke, and M. Ernzerhof, Generalized gradient approximation made simple, Phys. Rev. Lett. **77**, 3865 (1996).

[27] S. L. Dudarev, G. A. Botton, S. Y. Savrasov, C. J. Humphreys, and A. P. Sutton, Electron-energy-loss spectra and the structural stability of nickel oxide: An LSDA+ U study, Phys. Rev. B **57**, 1505 (1998).

[28] S. Baroni, S. De Gironcoli, A. Dal Corso, and P. Giannozzi, Phonons and related crystal properties from density-functional perturbation theory, Rev. Mod. Phys. **73**, 515 (2001).

[29] See Supplemental Material at https://xxxxxxxx for the detail of the calculations of D-tensor, the detail of the calculations of coherence time of quantum spin states, the charge density redistribution of Ir@C28 in phase I and II, schematic diagram of a conceptual two quantum spin system, and energy levels of two quantum spins as a function of exchange interaction strength, and two videos.

[30] H. W. Kroto, The stability of the fullerenes C_n, with n = 24, 28, 32, 36, 50, 60 and 70, Nature **329**, 529 (1987).

[31] X. D. Wang, R. Q. Wu, D. S. Wang, and A. J. Freeman, Torque method for the theoretical determination of magnetocrystalline anisotropy, Phys. Rev. B **54**, 61 (1996).

[32] J. Hu, and R. Q. Wu, Control of the magnetism and magnetic anisotropy of a single-molecule magnet with an electric field, Phys. Rev. Lett. **110**, 097202 (2013).

[33] R. Q. Wu, A. J. Freeman, Spin-orbit induced magnetic phenomena in bulk metals and their surfaces and interfaces, J. Magn. Magn. Mater. **200**, 498 (1999).

[34] H. Xiang, C. Lee, H. Koo, X. Gong, and M. Whangbo, Magnetic properties and energy-mapping analysis, Dalton Trans. **42**, 823 (2013).

[35] H. P. Breuer, The Theory of Open Quantum Systems (Oxford University Press, New York, **2007**).

[36] G. Stefanucci, and R. van Leeuwe, Nonequilibrium Many-Body Theory of Quantum Systems: A Modern Introduction (Cambridge University Press, New York, **2013**).

[37] S. Gómez-Coca, A. Urtizberea, E. Cremades, P. J. Alonso, P. A. Camón, E. Ruiz, and F. Luis, Origin of slow magnetic relaxation in Kramers ions with non-uniaxial anisotropy, Nat Commun. **5**, 4300 (2014).

[38] A. Lunghi1, F. Totti, R. Sessoli, and S. Sanvito, The role of anharmonic phonons in under-barrier spin relaxation of single molecule magnets, Nat Commun. **8**, 14620 (2017).

[39] L. Gu, and R. Q. Wu, Origins of slow magnetic relaxation in single-molecule magnets, Phys. Rev. Lett. **125**, 117203 (2020).

[40] M. Briganti, F. Santanni, L. Tesi, F. Totti, R. Sessoli, and A. Lunghi, A complete ab initio view of Orbach and Raman spin-lattice relaxation in a Dysprosium coordination compound, J. Am. Chem. Soc. **143**, 13633 (2021).

[41] D. Reta, J. G. C. Kragskow, and N. F. Chilton, Ab initio prediction of high-temperature magnetic relaxation rates in single-molecule magnets, J. Am. Chem. Soc. **143**, 5943 (2021).

[42] Y. Xu, J. S. Wang, W. Duan, B. L. Gu, and B. Li, Nonequilibrium Green's function method for phonon-phonon interactions and ballistic-diffusive thermal transport, Phys. Rev. B **78**, 224303 (2008).

[43] A. Ardavan, O. Rival, J. Morton, S. J. Blundell, A. M. Tyryshkin, G. A. Timco, and R. Winpenny, Will spin-relaxation times in molecular magnets permit quantum information processing? Phys. Rev. Lett. **98**, 057201 (2007).

[44] T. Almeida Murphy, T. Pawlik, A. Weidinger, M. Höhne, R. Alcala, and J. M. Spaeth, Observation of Atomlike Nitrogen in Nitrogen-Implanted Solid C_{60}, Phys. Rev. Lett. **77**, 1075 (1996).

[45] J. A. Larsson, J. C. Greer, W. Harneit, and A. Weidinger, Phosphorous trapped within buckminsterfullerene, J. Chem. Phys. **116**, 7849 (2002).

[46] W. Harneit, Spin Quantum Computing with Endohedral Fullerenes, Springer, Cham. (2017).